Improved Absolute Radiometric Calibration of a UHF Airborne Radar

Elaine Chapin*, Brian P. Hawkins*, Leif Harcke*, Scott Hensley*, Yunling Lou*, Thierry R. Michel*, Laila Moreira* †, Ronald J. Muellerschoen*, Joanne G. Shimada*, Kean W. Tham*, and Michael C. Tope*
* Jet Propulsion Laboratory, California Institute of Technology
4800 Oak Grove Dr., Pasadena, California 91109-8099
† Bradar Indústria S/A
Av. Shishima Hifumi, 2911 - sala 404
São José dos Campos, São Paulo 12244-000 Brazil

***Abstract*— The AirMOSS airborne SAR operates at UHF and produces fully polarimetric imagery [1]. The AirMOSS radar data are used to produce Root Zone Soil Moisture (RZSM) depth profiles. The absolute radiometric accuracy of the imagery, ideally of better than 0.5 dB, is key to retrieving RZSM, especially in wet soils where the backscatter as a function of soil moisture function tends to flatten out [2]. In this paper we assess the absolute radiometric uncertainty in previously delivered data, describe a method to utilize Built In Test (BIT) data to improve the radiometric calibration, and evaluate the improvement from applying the method.**

I. Introduction

An airborne ultra high frequency (UHF) synthetic aperture radar (SAR), designed to support root zone soil moisture (RZSM) retrievals, was built as part of the Airborne Microwave Observatory for Subcanopy and Subsurface (AirMOSS) project. The pod-based UHF radar was integrated and flight-tested with the NASA/Johnson Space Centers Gulfstream-III (G-III) aircraft in the summer of 2012 and has been operating since fall of 2012. We have conducted over 130 science flights with the radar over the AirMOSS projects study sites in North and Central America. The processed science data collected in 2012, 2013, and 2014 have been archived at Alaska Satellite Facility (ASF) and are freely available. The polarimetric phase is not calibrated for the data currently in the archive.

The techniques used to calibrate the SAR data lean heavily on those used to calibrate AIRSAR, GeoSAR, and UAVSAR [3], [4], [5], [6]. In this paper, we assess the radiometric calibration accuracy of the currently archived data and discuss improvements to the calibration. These improvements will be applied to new data collected and to data collected after April 2013 when those raw data are reprocessed.

II. Assessment

We assess the quality of our radiometric calibration by imaging approximately 26 smaller (2.4 m) trihedral corner reflectors and 5 larger (4.8 m) trihedral corner reflectors deployed at Rosamond Dry Lake in California [7]. Figure 1 is an AirMOSS image of the Dry Lake collected on a northbound flight. By comparing the measured backscatter with the predicted backscatter, we determined that our absolute radiometric error was approximately ± 1 dB. This absolute calibration estimate was using an initial antenna pattern and utilizing none of the radar's internal calibration signals for radiometric correction. Figure 2 shows typical corner reflector performance.

Although not as quantitative, we also use the AirMOSS data collected at the science sites to look for data-takes whose radiometric offset is inconsistent with previous observations of the same scene. For AirMOSS, we image the same 10 science sites repeatedly, flying each site 3 to 9 times per year depending on the site. We binned the backscatter data versus incidence angle to derive curves characteristic of various sites. We could detect potential calibration errors when the curve for an individual data-take differed significantly (e.g., more than predicted by RZSM and vegetation models) from the other collections. For example, Figure 3 shows evidence of gain biases.

III. Built-in-Tests

Before each data-take, the radar collects a few minutes of data from a set of five Built-in-Tests (BITs):

1) receive-only sniffer pulses where the receiver is active but the transmit chain is not,
2) full-chain calibration pulses where the radar's chirp is routed through the transmit and receive chains but not out the antenna or through some passive components in the front-end,
3) partial-chain calibration pulses where the radar's chirp is routed through much of transmit and receive chains but excludes the high power amplifier,
4) receiver test data where the receiver looks not at the antenna but at a resistive load, and
5) receiver test data where the receiver looks not at the antenna but at a built in noise diode.

A typical data-take is 15 minutes long. A single calibration pulse of the first three types above are collected approximately every 10 seconds within the data-take. The same set of five BITs performed before the data-take is collected again after each data-take.

We investigated whether the BITs are correlated with the absolute radiometric error using 26 southbound data-takes

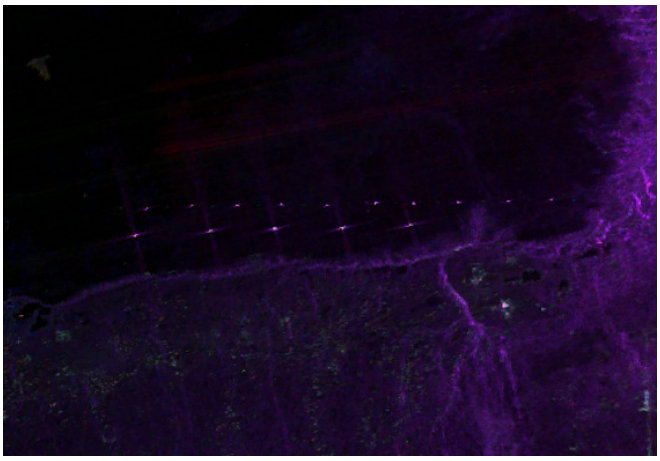

Fig. 1. Imagery of Rosamond Dry Lake showing 13 of the smaller corner reflectors, 5 of the larger corner reflectors, and the edge of the lakebed. The lakebed is deliberately chosen for its low backscatter.

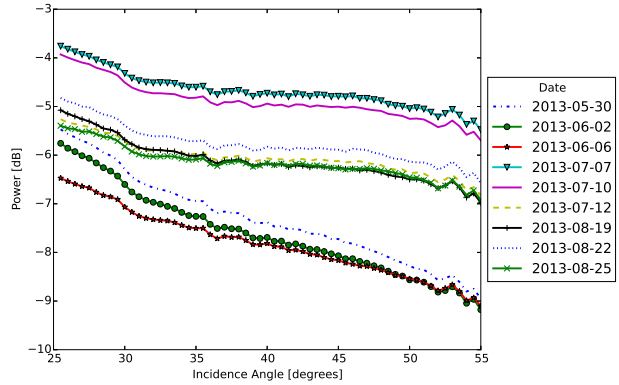

Fig. 3. HH Backscatter curves for various 2013 data acquisitions at Howland Forest, ME. Note the two curves from July (13-07-07 and 13-07-10) that seem much higher than the rest.

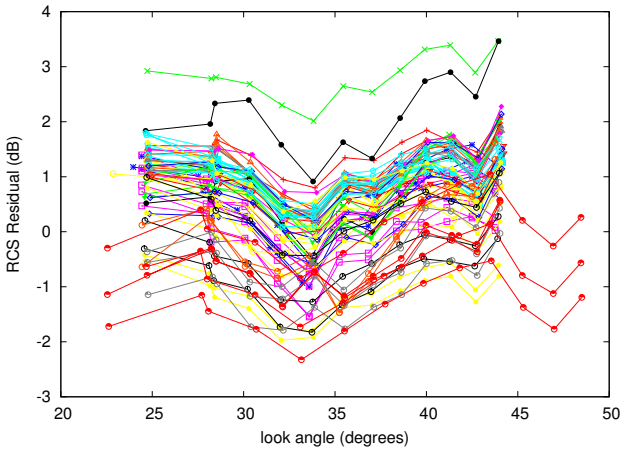

Fig. 2. Plot showing the HH polariztion radar cross section residual for the 13 smaller corner reflectors as a function of look angle. Each different colored curve corresponds to a different data-take.

imaging Rosamond Dry Lake in 2014. All of these data-takes view the corner reflectors with similar geometry except for squint resulting from the variable yaw of the aircraft. For each data-take, we calculated the average radiometric error for the data-take using the corner reflectors. We then calculated the relevant power parameter for the ten BITs associated with that data-take and looked for correlations. For the HH channel data, for example, we found a 95% correlation between the average post-data-take full-chain calibration pulse power and the radiometric error. An 89% correlation was found between the average post-data-take noise diode power and the radiometric error. Figures 4 and 5 show examples of the noise diode data and the corner reflector residuals relationship.

The high correlation for the full-chain calibration pulse power was expected since it covers almost the entire electronics chain. The high correlation for the noise diode test - which excludes the entire transmit chain including the high power amplifier which does not operate in saturation - comes because the root cause of the radiometric variability of all of the electronics is temperature.

IV. Noise Diode Based Correction

We decided to use the noise diode BIT data in order to calculate our radiometric correction. One factor in the decision was the stability of the noise diode BIT. Over the years of radar operations, we have repeatedly improved the hardware and changed the parameters used for the BITs. For example, the hardware for the full-chain calibration pulses was changed in July 2014. The noise diode, however, has not changed significantly since April 2013. Consequently, a correction that utilizes the noise diode BIT allows for more legacy data to be reprocessed.

We calculated a radiometric correction model that is applied to each data-take. Figures 4 and 5 show the residual corner reflector power as a function of the average noise diode BIT power. Each point represents the residual averaged over all 13 smaller corner reflectors imaged in a single data-take. All of the southbound data collected at Rosamond Dry Lake between July 2013 and October 2014 appear in the plot. The points shown in Figures 4 and 5 were then fit with a line, also shown in the Figures. The slope of this line and the noise diode BIT data for an individual data-take are used to calculate the radiometric correction for that data-take.

After the radiometric correction model was calculated, we reprocessed the northbound data collected at Rosamond Dry Lake between July 2013 and October 2014 applying the correction. The larger corner reflectors, which appear in the northbound data, were used to calculate updated radar calibration parameters to zero the overall radiometric bias. The larger reflectors are used for the bias estimation since their multiple wavelength size makes them closer to the ideal corner reflector model.

V. Results

All of the Rosamond Dry Lake data after June 2013 have been reprocessed with the updated radiometric calibration

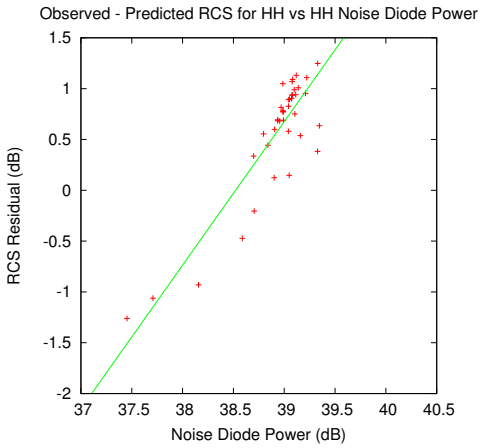

Fig. 4. Plot of the average residual corner reflector power as a function of the average noise diode BIT power for HH channel data.

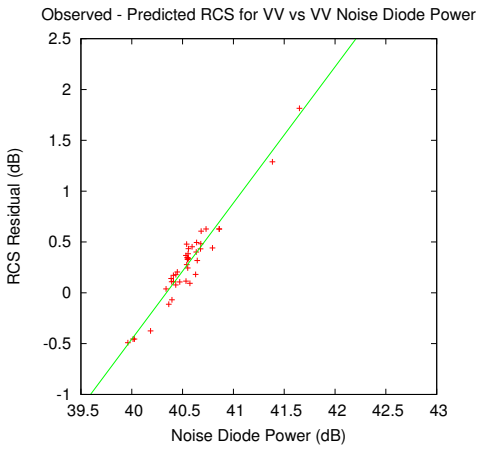

Fig. 5. Same as Figure 4 for the VV channel.

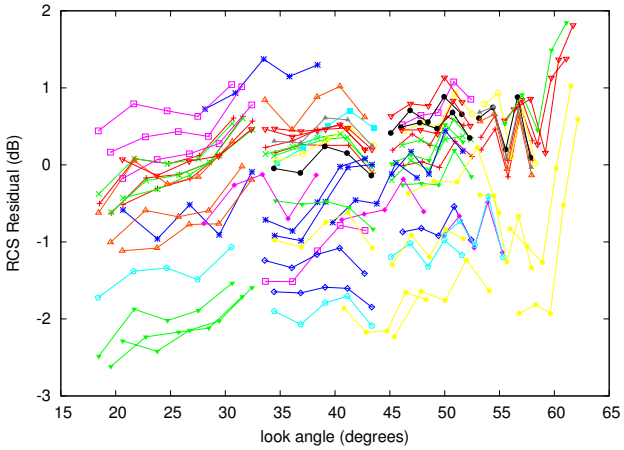

Fig. 6. Plot of the residual corner reflector power as a function of look angle for the 4.8 m reflectors imaged in the HH channel data when no noise diode BIT based correction is included. Each curve corresponds to a different data-take. Each color corresponds to a different flight.

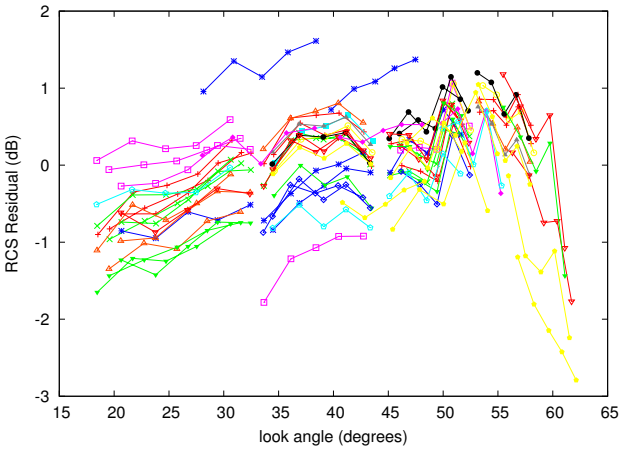

Fig. 7. Same as Figure 6 for the VV channel.

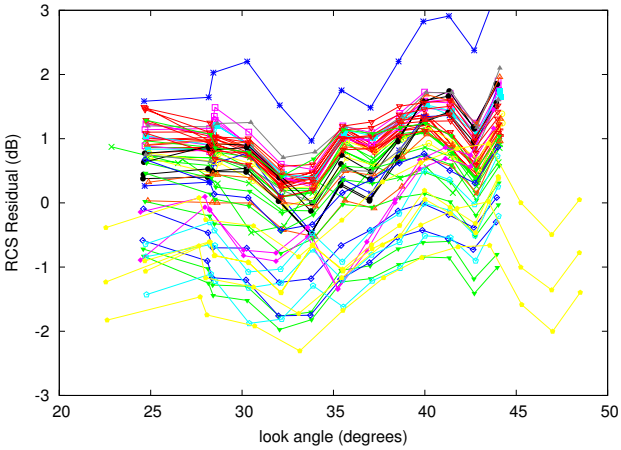

Fig. 8. Same as Figure 6 for the 2.4 m reflectors.

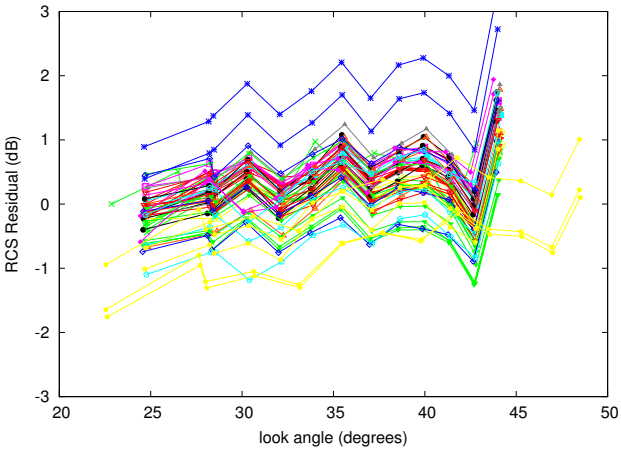

Fig. 9. Same as Figure 7 for the 2.4 m reflectors.

	Uncorrected Mean (dB)	Corrected Mean (dB)	Uncorrected Sigma (dB)	Corrected Sigma (dB)
HH 4.8 m	N/A	N/A	0.867	0.543
HH 2.4 m	+0.433	+0.547	0.861	0.564
VV 4.8 m	N/A	N/A	0.668	0.521
VV 2.4 m	+0.251	+0.240	0.599	0.436

TABLE I

IMPROVMENT IN THE MEAN AND STANDARD DEVIATION OF THE CORNER REFLECTOR RESIDUALS WHEN THE NOISE DIODE BIT CORRECTION IS APPLIED

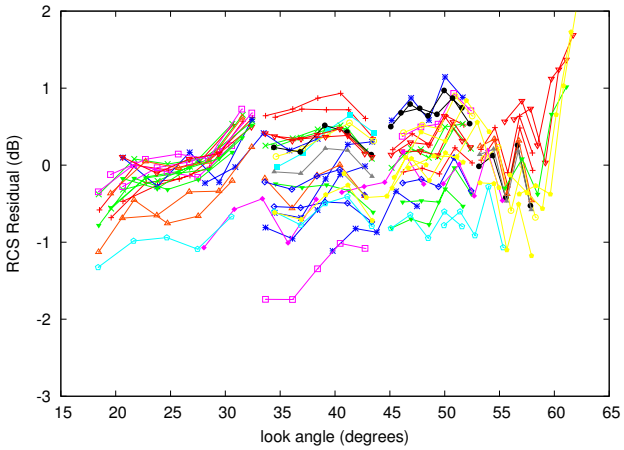

Fig. 10. Plot of the residual corner reflector power as a function of look angle for the 4.8 m reflectors imaged in the HH channel data when the noise diode BIT based correction is included. Each colored curve corresponds to a different data-take.

parameters and using the noise diode BIT derived offsets. Figures 6 through 9 show the corner reflector residuals without these calibration enhancements, and Figures 10 through 13 show the residuals with the enhancements applied. The spread of the corner reflector residuals is reduced. Table I summarizes the results. In Figures 6 through 13, the plots of the 4.8 m reflectors include all of the northbound Rosamond data-takes collected from July 2013 through February 2015, and the plots of the 2.4 m reflectors include all of the southbound data from the same period.

Although the noise diode BIT based correction improves the calibration, there are still issues. In particular, there are still outliers, such as the isolated data-take shown in pink in Figure 11. Analysis such as that shown in Figure 3 is recommended for users of the data who care about the absolute radiometric bias of their scenes.

VI. ANTENNA PATTERN

Another avenue for improving the radiometric accuracy is improving the antenna pattern. The effective pattern of the AirMOSS system is strongly impacted by the wing of the aircraft because of its proximity to the antenna [1]. This interaction was simulated in a computational electromagnetic model, but the model results did not match observed data. An alternate antenna gain measurement procedure was designed

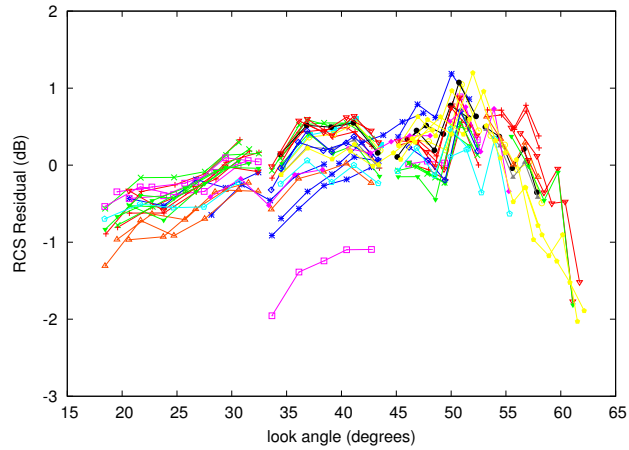

Fig. 11. Same as Figure 10 for the VV channel.

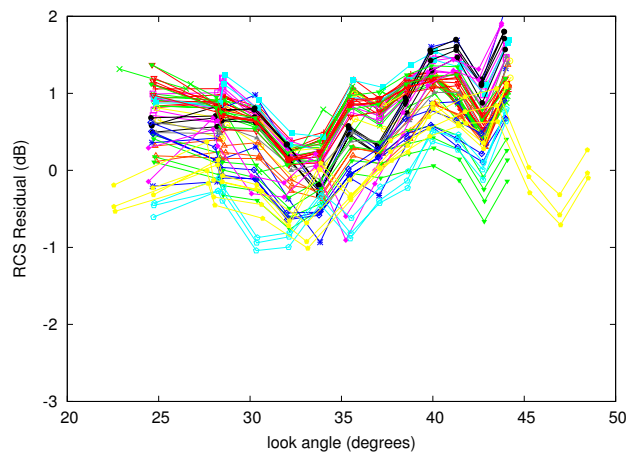

Fig. 12. Same as Figure 10 for the 2.4 m reflectors.

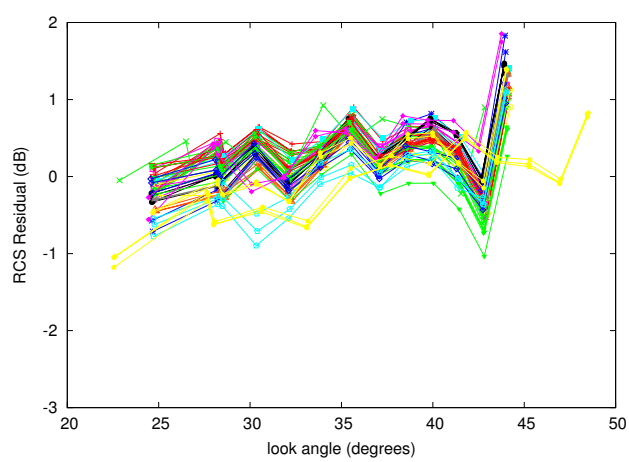

Fig. 13. Same as Figure 11 for the 2.4 m reflectors.

using the range compressed data. The backscattered power of each of the larger corner reflectors for each of the data-takes was measured as the corner reflectors walked through the beam. The antenna gain in direction cosine U/V space was derived by model regression, using the observed backscattered power as a function of position measurements and the radar equation.

An initial version of the antenna pattern using this method was made in 2012 using early AirMOSS data. One challenge in combining the curves from various data-takes together was the data-take to data-take radiometric variability which was estimated along with the antenna pattern parameters. We have re-estimated the antenna pattern using the BIT data to take out the radiometric variability instead of estimating it. Figure 14 shows cuts through the updated antenna pattern.

Our method of estimating the antenna pattern relies on high signal-to-noise ratios for the corner reflectors. Although Figures 6 through 13. show the corner reflector residuals at large angles, data with look angles past 55° are not delivered since the antenna pattern is too uncertain at large look angles. In the future, we could collect additional data-takes imaging the larger corner reflectors at large angles while flying at lower altitudes to extend the antenna pattern.

The updated antenna pattern was used for all of the data shown in Figures 6 through 13. Repeatable patterns can be seen in the corner reflector residuals for the 2.4 m reflectors. For example, the VV data shows a sharp knee and high values at approximately 44° look angle corresponding to the farthest range reflector. The structure seen in the plots of the residuals for the 2.4 m reflectors does not reflect errors in the antenna pattern. Instead, it reflects differences in the actual corner reflectors themselves. These smaller reflectors were deployed decades ago. Different reflectors have suffered different degradation over the years. These reflector-to-reflector differences are highlighted by the yellow curves in Figures 12 and 13 which were flown at with a displaced flight trajectory from the rest of the data-takes in the plot. These curves show the same basic pattern of high and low values only they are spread over a different look angle range.

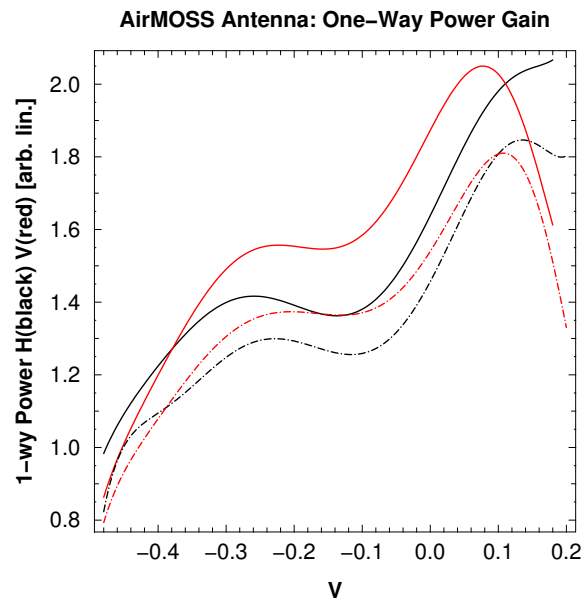

Fig. 14. Look angle cuts through updated antenna pattern. The original pattern are the dash-dotted curves; the updated pattern are the solid curves. The black curves are HH; the red curves are VV. The abscissa V is the direction cosine with the short axis of the rectangular antenna face. V increases with look angle.

VII. Conclusion

The data from the AirMOSS radar have been used to retrieve soil moisture successfully [8]. However, the retrieval quality and the ease of doing the retrieval could be enhanced with better radiometrically calibrated data. We have re-estimated our antenna pattern and have developed a method to utilize our BITs for each data-take to improve the data products. New data and older reprocessed data added to the AirMOSS archive at ASF will reflect these improvements.

Acknowledgment

The work reported here was performed at the Jet Propulsion Laboratory, California Institute of Technology, under contract with the National Aeronautics and Space Administration.

References

[1] E. Chapin, A. Chau, J. Chen, B. Heavey, S. Hensley, Y. Lou, R. Machuzak, and M. Moghaddam, "AirMOSS: An airborne P-band SAR to measure root-zone soil moisture," in *2012 IEEE Radar Conference (RADAR), Atlanta, GA*, May 2012, pp. 0693–0698.

[2] A. Tabatabaeenejad and M. Moghaddam, "Radar retrieval of surface and deep soil moisture and effect of moisture profile on inversion accuracy," *Geoscience and Remote Sensing Letters, IEEE*, vol. 8, no. 3, pp. 478–482, May 2011.

[3] E. Chapin, S. Hensley, and T. Michel, "Calibration of an across track interferometric P-band SAR," in *Geoscience and Remote Sensing Symposium, 2001. IGARSS '01. IEEE 2001 International*, vol. 1, 2001, pp. 502–504 vol.1.

[4] Y. Kim and J. van Zyi, "Polarimetric and interferometric SAR calibration verification methods," in *Geoscience and Remote Sensing Symposium, 2001. IGARSS '01. IEEE 2001 International*, vol. 3, 2001, pp. 1098–1100 vol.3.

[5] A. Chu, Y. Kim, J. Van Zyl, Y. Lou, and B. Chapman, "The interferometric data calibration for the AIRSAR PacRim II mission," in *Geoscience and Remote Sensing Symposium, 2005. IGARSS '05. Proceedings. 2005 IEEE International*, vol. 3, July 2005, pp. 2098–2100.

[6] A. Fore, B. Chapman, B. Hawkins, S. Hensley, C. Jones, T. Michel, and R. Muellerschoen, "UAVSAR polarimetric calibration," *Geoscience and Remote Sensing, IEEE Transactions on*, vol. 53, no. 6, pp. 3481–3491, June 2015.

[7] A. H. Chau, E. Chapin, A. Ceniceros, B. Heavy, S. Hensley, Y. Lou, R. Machuzak, M. Moghaddam, R. Muellershoen, R. van Schilfgaarde, and K. C. Wang, "AirMOSS P-band SAR calibration," in *CEOS SAR Calibration and Validation Workshop, Fairbanks, AK, Nov 7-9 2011*, Nov 2011.

[8] A. Tabatabaeenejad, M. Burgin, X. Duan, and M. Moghaddam, "P-band radar retrieval of subsurface soil moisture profile as a second-order polynomial: First AirMOSS results," *Geoscience and Remote Sensing, IEEE Transactions on*, vol. 53, no. 2, pp. 645–658, Feb 2015.